ACS APPLIED NANO MATERIALS
Cite This: ACS Appl. Nano Mater. XXXX, XXX, XXX−XXX
Article
www.acsanm.org

Atomic Layer Deposition Tuning of Subwavelength Aluminum Grating for Angle-Insensitive Plasmonic Color

Daniel Franklin,*[,†,‡] Matthew George,[§] James Fraser,[§] and Debashis Chanda*[,†,‡,∥]

[†]Department of Physics, University of Central Florida, 4111 Libra Drive, Physical Sciences Bldg. 430, Orlando, Florida 32816, United States

[‡]NanoScience Technology Center, University of Central Florida, 12424 Research Parkway, Suite 400, Orlando, Florida 32826, United States

[§]MOXTEK, Inc., 452 W 1260 N, Orem, Utah 84057, United States

[∥]CREOL, The College of Optics and Photonics, University of Central Florida, 4304 Scorpius St., Orlando, Florida 32816, United States

Supporting Information

ABSTRACT: The angle-insensitive and tunable nature of metal−insulator−metal slits makes them an interesting candidate for plasmonic displays and colorant applications. The realization of these structures in the visible regime and over reasonably large areas has only been recently possible due to advances in nanofabrication. However, previous demonstrations are of inverted grooves etched into a dielectric, coated with a metal and then probed from the substrate—leaving them unable to be tuned postfabrication, as the regions of confined fields become inaccessible. Second, these demonstrations use area and time-limited fabrication processes such as EBL or FIB milling. Here, we demonstrate 8 in. wafer scale angle-insensitive plasmonic color through vertical metal−insulator−metal slit waveguides in which the resulting resonances can be accessed and tuned through external media. To illustrate this, we use atomic layer deposition to change the effective refractive index of the surrounding media and tune resonance locations throughout the entire visible regime. The tunable single-peak absorption resonance results in the reproduction of the cyan, yellow, and magenta (CYM) color space. The system's angle insensitivity and large scale allow the creation of polarization-dependent images and logos which can find use in novel plasmonic optical components and further demonstrate the potential of such systems to be integrated with dynamically tunable optical media.

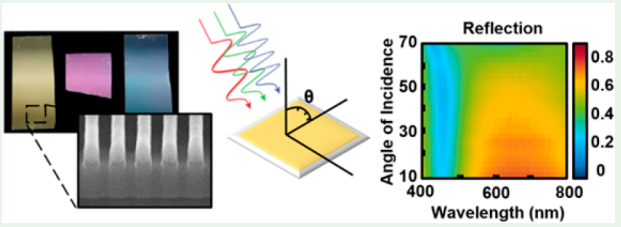

KEYWORDS: *plasmonics, structural color, aluminum, angle-insensitive color, color tuning, displays, ALD*

INTRODUCTION

Metal nanostructures have been shown to produce diffraction limited color which can potentially lead to the smallest possible color pixels[1]—an increasingly important property given the resolution requirements of next-generation mobile and head mounted displays. Perhaps even more impressive is the ability to tune the optical resonances of metal nanostructures postfabrication through control of external and surrounding media. This has been used to create dynamic color changing surfaces[2−10] as well as colorimetric sensors and detectors.[11−13] Viewing angle dependence is a vital figure of merit for many of these applications including consumer goods coloration, displays, and camouflage—all of which require the viewer to see the desired image content regardless of orientation. However, not all structural color generating nanostructures have angle-independent coupling mechanisms. In the case of photonic crystals, the evolution of bird feathers shows a possible solution. Iridescence in bird feathers is attributed to the fundamental angle dependence of periodic nanostructures existing within their barbules. However, many species including macaws have evolved bright noniridescent colors by incorporating controlled randomness into the nanostructures.[14−16] Rather than being perfectly periodic, the organic photonic crystals exhibit a short-range order needed for Bragg reflection but lack long-range order. This results in an averaging effect and an effective band gap, which reflects a specific wavelength of light for all angles. This compensational approach of engineered randomness has also been demonstrated in man-made photonic crystals[17−19] and plasmonic structures.[20−22] An alternative approach toward angle-independent color filters has been demonstrated through layers of thin metals and dielectrics. By depositing a metal/dielectric and then another layer of a metal, the system can support Fabry−Perot resonances, which absorb or transmit light based on constructive or destructive interference. Differences in the path length of light for varying incidence

Received: July 19, 2018
Accepted: August 14, 2018
Published: August 14, 2018

DOI: 10.1021/acsanm.8b01147
ACS Appl. Nano Mater. XXXX, XXX, XXX−XXX

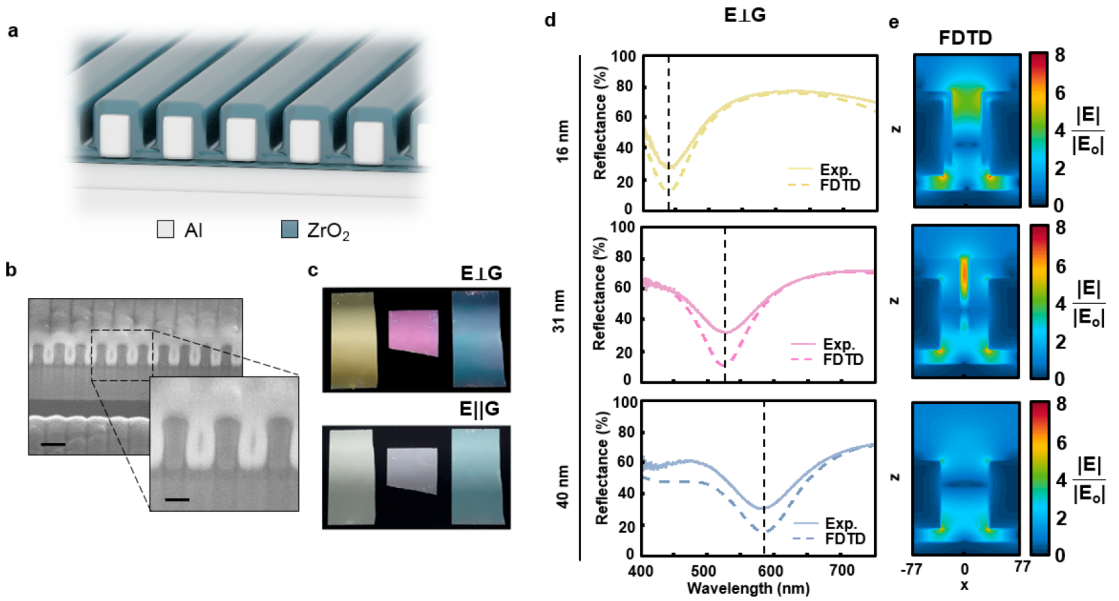

Figure 1. Subwavelength plasmonic resonator and mode of operation. (a) Schematic of the 1D aluminum wires separated from an aluminum mirror by a thin oxide. Coating the structure with uniform conformal films of oxide allows shifting of plasmonic resonances. (b) Scanning electron microscope image of a focused ion beam cross section of the plasmonic system coated with 42 nm of ZrO_2. Scale bars are 140 nm and 70 nm, respectively. (c) Camera images of three samples coated with a selected thickness of ZrO_2 to give yellow magenta and cyan, respectively. Top image is for polarization of light perpendicular to the aluminum wires while the bottom image is for polarization parallel to the aluminum wires. Yellow and cyan samples are 1 inch tall. (d) Reflectance spectra of the samples shown in (c) with supporting finite difference time domain simulated spectra. (e) Field profiles of the electromagnetic field at resonance (dotted black line of (d)) within a unit cell of the plasmonic structure.

angles commonly make these systems highly angle dependent.[23] However, researchers have found a way to compensate for this variance by engineering the angle-dependent phase of reflection.[24−28] This method requires the use of specific metals/dielectrics and thickness combinations for a desired resonance wavelength and therefore can be highly restrictive. Furthermore, attempts at incorporating active tuning can negate the precise phase conditions and lose system angle independence.

Another approach toward angle-independent color filters is to use inherent angle-insensitive coupling mechanisms which exist in subwavelength systems.[29,30] The optical modes of metal−insulator−metal waveguides has long been an area of study—often focused on their interactions with light much larger than their physical dimensions and the intensely confined fields they generate.[31−33] This property of enhanced near-field confinement led to the fundamental study of such modes, detailing analytic field profiles and resonance conditions.[34−41] More recently, researchers have focused on another aspect of such structures—angle-insensitive coupling with incident light.[42−44] The origin of this insensitivity has been rationalized through analysis of the EM field near the surface, which shows oscillations in charge density near the top corners of the metallic grooves. These effectively act as radiating dipoles and function as coupling mechanisms for incident light into the metal−insulator−metal waveguide. The excitation of these localized plasmons is highly angle-insensitive, making the combined slit Fabry−Perot resonator angle-insensitive as well. Lastly, the resonances of a surface containing metal−insulator−metal slits or grooves have been shown to behave as an array of independent subwavelength resonators. In other words, a surface containing only a singular slit will also resonant and absorb light based on its optical cross section. This individual resonator behavior and subwavelength nature result in a diffraction-less system in which the phase profile and wavefront of reflected light are uniform and mirror-like.

The angle-insensitive nature of metal−insulator−metal slits makes them an interesting candidate for color filter technology, while their sensitivity to external media may lead to unique plasmonic displays and devices. The realization of these structures in the visible regime and over reasonably large areas has only been recently possible due to advances in nanofabrication. However, previous demonstrations are of inverted grooves etched into a dielectric, coated with a metal and then probed from the substrate.[42] Resonators made this way are unable to be tuned post-fabrication as the regions of confined fields are inaccessible. Second, these demonstrations use area and time-limited fabrication processes such as EBL or FIB milling. Here, we demonstrate 8 in. wafer scale angle-insensitive plasmonic color through optical interference lithography, in which the resulting resonances can be accessed and tuned through external media. The ability to tune the resonators, postfabrication, leverages a key advantage of plasmonic systems and could lead to dynamic optical components for displays and sensors. To illustrate this, we use atomic layer deposition to change the effective refractive index of the surrounding media to tune resonance location throughout the entire visible regime. The tunable single absorption resonance results in the reproduction of the cyan, yellow, and magenta (CYM) color space. We validate the system's angle insensitivity through angle-resolved integrating sphere measurements and last show the ability to pattern a single surface with varying thickness of ALD-coated zirconium oxide (ZrO_2) to create patterns, images, and logos.

DOI: 10.1021/acsanm.8b01147
ACS Appl. Nano Mater. XXXX, XXX, XXX−XXX

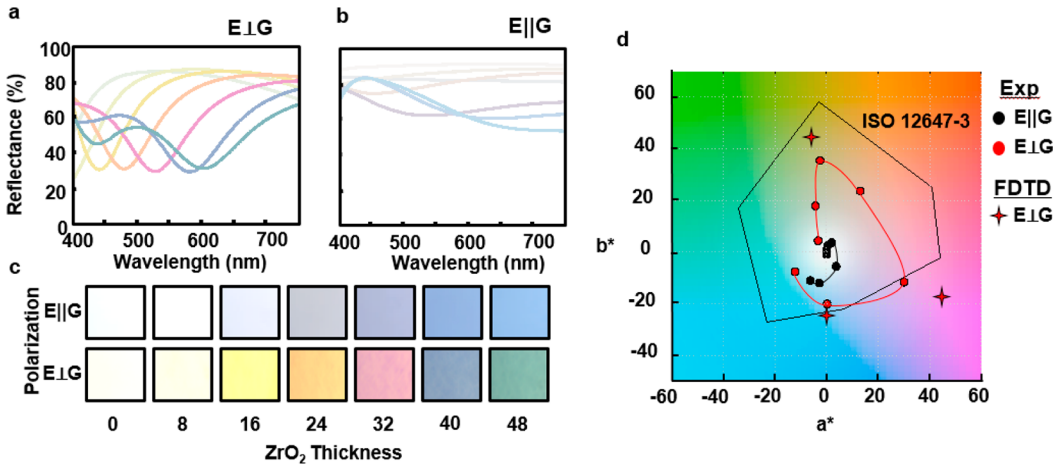

Figure 2. Atomic layer deposition dependent structural color. (a) Reflectance spectra of the subwavelength plasmonic system as a function of ZrO_2 thickness for light polarized perpendicular to the aluminum wires. Resonances continuously red-shift with increasing thickness. (b) Reflectance spectra excited with the orthogonal polarization. Spectra largely remains flat and uniform. Line colors are obtianed through the CIE color matching functions. (c) Microscope images corresponding to the thicknesses and polarizations of (a, b). (d) CIE LAB chromaticity diagram depicting the color quality of the surfaces as a function of thickness and polarization. Color quality can be compared to that of standard CYM print on newspaper, ISO 12647-3.

RESULTS

Aluminum Plasmonic Surface. The plasmonic metal−insulator−metal surface consists of a 1D aluminum grating separated from an aluminum mirror by a thin 10 nm SiO_2 dielectric spacer. The structure is fabricated by performing photolithography atop a stack of thick aluminum, 10 nm oxide, and a 100 nm film of aluminum. The system is then etched to create deep slits in the top layer of aluminum, where the thin oxide layer performs as an etch stop. After the etch mask is removed, the now electrically floating aluminum wires can be coated and tuned through external media. The structure hosts a metal−insulator−metal resonance between the gaps of the aluminum wires which strongly absorbs light at a given resonant wavelength. This resonant wavelength is dependent on the Fabry−Perot condition of a vertically propagating electromagnetic wave within the slot waveguide and is contingent on the height and width of the aluminum wires along with the surrounding media's refractive index. By depositing a continuous ALD oxide film, the effective refractive index within the wire grid can be modified, which results in a continuous tuning of the structure's resonance wavelength. A schematic and focused ion beam milled cross section of the wire grid after being coated with 42 nm of ZrO_2 are shown in Figures 1a and 1b, respectively. The period of the structure is 144 nm, with a width of 80 nm and depth of 100 nm. These structural dimensions are chosen so that the system supports resonances in the visible regime when coated with materials of refractive index between 1.5 and 2. By coating the structure with thin films of a high index oxide, an effective index of between the chosen oxide and air is achieved. For this reason, we chose ZrO_2 ($n \sim 2.15$) as our coating oxide though other high index oxides such as TiO_2 and HfO_2 could also be used. Figure 1c shows three samples with selected ZrO_2 thicknesses to obtain yellow (15 nm), magenta (27 nm), and cyan (42 nm). The 1D nature of the wire grid creates a polarization-dependent resonance which determines the corresponding reflection spectrum. When imaged through a polarizer perpendicular to the grating, colors are clearly seen. However, the orthogonal polarization (parallel to the grating) fails to couple to the metal−insulator−metal resonance, reflecting a uniform spectrum of light and producing a mirror-like surface. Corresponding reflectance measurements of the surfaces are shown in Figure 1d for light incident perpendicular to the wires. Line colors are obtained from the CIE chromaticity functions, and dotted lines indicate a qualitative match to spectra obtained through FDTD simulations. Adjacent to this, Figure 1e depicts the field profile of the electromagnetic field about the structures at resonance for the respective oxide thicknesses.

This resonance condition is given simply by

$$\left(\frac{1}{4} + \frac{1}{2}m\right)\lambda = n_{\text{eff}}D$$

where D is the depth, n_{eff} is the effective refractive index within the resonator, λ is the resonant wavelength, and m is the order of the resonance.[42] Absorption and standing waves occur within the grooves analogous to the quarter-wave condition of Fabry−Perot resonators. However, the system varies slightly than the case for which this resonance condition was derived due to the existence of the etch stop layer. This oxide effectively increases the depth of the resonator as well as electrically separates the wires from the aluminum mirror. From the field profiles shown in Figure 1e, we see this isolation results in the localization of plasmonic fields on the bottom corners of the aluminum wires. Because of this, the system resonances resemble a hybrid between that of a pure metal−insulator−metal slit waveguide and that of a metal particle near-field coupled to a mirror. Despite this difference, Figure 1 clearly shows the existence of these resonances and the structural color that follows.

Color Tuning through Oxide Thickness. To continuously tune the resonances of the aluminum subwavelength resonators, we coat the structures with a continuous and conformal layer of zirconium oxide. This is performed through atomic layer deposition, which allows precise control of the deposited material thickness. The refractive index and thickness of a given oxide will depend on deposition conditions (Supporting Information Figure S1 shows the optical properties and growth rate of the ALD ZrO_2). Figure 2a,b shows the reflection spectra of the surface as a function of ZrO_2 thickness

DOI: 10.1021/acsanm.8b01147
ACS Appl. Nano Mater. XXXX, XXX, XXX−XXX

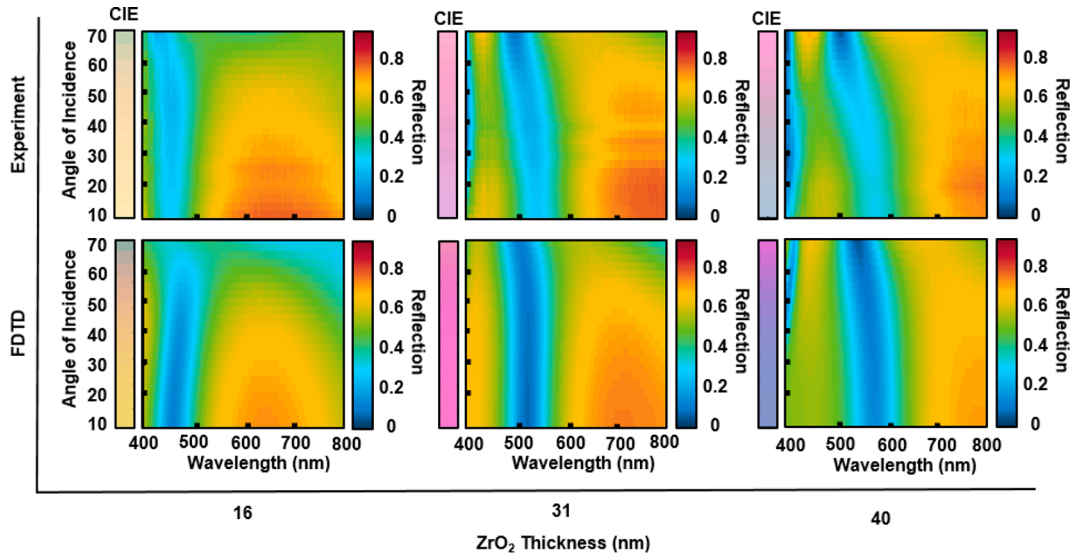

Figure 3. Angle dependence of the plasmonic surface. Top row depicts the experimentally obtained reflectance spectra of the surface as a function of angle and ZrO_2 thickness. The bottom row contains the finite difference time domain simulations of the surface. Experiment and simulation are both performed for incident light-polarized perpendicular to the aluminum wires and therefore exciting the metal−insulator−metal Fabry−Perot resonance. Adjacent to each data set is the CIE predicted color given the reflection spectrum of the surface at the respective angle.

and polarization of incident light. A linear relation between oxide thickness and resonance location is observed up to the point where the aluminum gap is filled. This occurs when depositing a thickness roughly half of the aluminum rib gap (in this case ∼32 nm). Line colors are obtained through the CIE chromaticity matching functions and match closely to camera images obtained through a microscope with a 10× objective (Figure 2c) for each of the oxide thicknesses and both orthogonal polarization states. Lastly, the resulting colors can be evaluated through the CIE chromaticity diagram in Figure 2d. For comparison, we overlaid the ISO 12647-3 color space standard for subtractive color printing on newsprint on the CIE chromaticity diagram. Despite being able to widely tune and spectrally place the structural resonance, the absorption of 60−70% and the corresponding reflection of ∼30% result in unsaturated pastel-like colors. This deviates from the FDTD simulations of Figure 1d which predict deeper resonances approaching 95% absorption. To see the difference in color this produces, we also plot the CIE coordinates of the simulated spectra for the yellow, magenta and cyan samples in Figure 2d. Despite resulting in a wider gamut, the difference between simulation and experiment on the CIE coordinates is relatively small given 25% difference in absorption between simulation and experiment. This highlights the nonlinear nature of the CIE algorithm and the importance of achieving near-perfect absorption to realize large subtractive color spaces. We believe the color performance of both the simulated and experimental spectra is achievable through further parameter optimization.

We attribute differences between simulation and experimental spectra to variations in structure parameters and roughness of the etched aluminum, which can all lead to increased scattering and a decreased quality factor of the experimentally fabricated pattern. Slight differences may also be due to the exposure of the aluminum structure to the elevated temperature of the reaction chamber. While the reaction is performed at 150 °C, well below the melting point of aluminum at 660 °C and eliminating the potential for direct deformation, the dynamics of the native aluminum oxide layer do depend on temperature and exhibit several growth modes.[45] Below 300 °C, an amorphous layer of oxide forms which is thickness-limited within the range of 2−5 nm. From this we hypothesize that the change in native oxide thickness from room temperature to the reaction temperature would be on the order of 1−2 nm. Through numerical simulation, this decrease in aluminum wire size and increase in oxide thickness correlates to a one-time shift in resonance wavelength between 5 and 10 nm.

Angle Dependence. Figure 3 shows the angle-resolved reflectance spectrum of the three selected CYM samples of Figure 1. Experimental measurements and simulations both show relative degrees of angle insensitivity over a 70° span. The yellow (16 nm), magenta (31 nm), and cyan (40 nm) samples exhibit a 20, 50, and 65 nm shift in resonance location across a 70° span. To show the impact of these shifts on the perceived color of the surface, we provide the CIE predicted color next to each measurement and simulation. From this we find that the yellow (16 nm) and magenta (32 nm) samples are largely color invariant up to 60°−70°, whereas the cyan (40 nm) sample begins to shift from cyan to magenta at ∼50°. Interestingly, as the viewing angles of the samples increase, so too does the resonant absorption of the magenta (32 nm) and cyan (40 nm) samples. This pronounced increase in absorption greatly increases the color quality produced by the structure. However, this effect is not observed in the ideal FDTD simulation case. We interpret this as the resonance being less sensitive to errors in fabrication for higher angles of incident light.

Detailed previous studies have found that the choice of periodicity is vitally important to realize angle-insensitive absorption.[46] Multiple plasmonic modes can exist for a system, and care must be taken not to excite those dependent on periodic features. Periodicities above 200 nm exhibit a grating coupled plasmon resonance and can intersect and interfere with angle-insensitive metal−insulator−metal Fabry−Perot resonances. Below 100 nm, however, the desired metal−insulator−metal resonances are no longer supported. The ideal periodicity for their specific structure was shown to be ∼180

DOI: 10.1021/acsanm.8b01147
ACS Appl. Nano Mater. XXXX, XXX, XXX−XXX

nm for a surrounding index equivalent to quartz.[42] Fabrication constraints have limited us to 144 nm periodicities, but the above results show that this is still adequate to demonstrate angle insensitivity up to 70°. Again, we believe it is possible to improve the color and angle performance of the system through further parameter optimization.

Image Formation. The proposed plasmonic system and method by which it is fabricated also holds several key advantages compared to previous demonstrations. Above, we have shown how resonances can be controlled through the deposition of external media, in contrast to the inverted and inaccessible grooves of previous fabrication methods. The method used here is also CMOS compatible, which allows fabrication over large areas compared to electron-beam lithography or focused-ion-beam approaches. Figure 4a shows camera images of the plasmonic surface over an 8 in. wafer for both polarization states. The grating has been coated with a thin layer of oxide to shift the plasmonic resonance to 450 nm, producing a yellow for one polarization state while maintaining the white color of a mirror for the corresponding orthogonal polarization. Lastly, since this color depends on the thickness of oxide deposited on the uniform gratings, images and logos can be formed through standard UV lithography and lift-off techniques. Figure 4b shows the UCF Pegasus logo patterned through this method. For incident light polarized parallel to the subwavelength grating, the surface appears in gray scale. However, perpendicularly polarized light excites the Fabry–Perot metal–insulator–metal waveguide mode and results in the desired colored image, where the logo appears in magenta on a yellow background. Subsequent patterning and ALD depositions can give images with cyan as well covering the whole CYM color space.

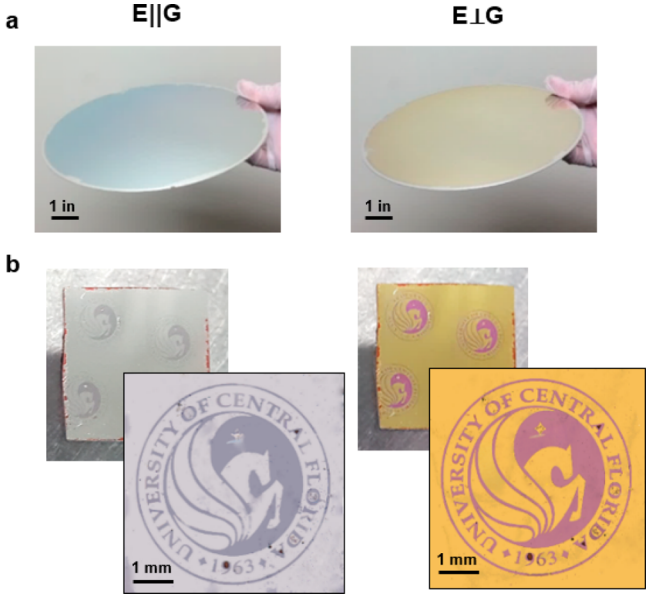

Figure 4. Wafer scale production and image formation. (a) Camera images of an 8 in. diameter wafer supporting the subwavelength plasmonic structure. The structure is coated with a thin film of oxide to produce a yellow reflectance when polarized perpendicular to the aluminum wires and a white mirror reflectance when parallel. (b) Demonstration of the patterned thickness variations to achieve polarization sensitive and colored logos. Sample is patterned through a series of depositions and lift-off procedures.

DISCUSSION

In summary, we have demonstrated wafer scale, angle-insensitive plasmonic color in which the resulting resonances can be accessed and tuned through external media. To illustrate this, we used atomic layer material deposition of ZrO_2 to change the effective refractive index of the surrounding media and tune the resonance location throughout the entire visible regime. Tuning of this single absorptive resonance results in the reproduction of the cyan, yellow, and magenta (CYM) color space. We quantify the system's angle insensitivity through angle-resolved integrating sphere measurements and last show the ability to pattern a single surface with varying thickness of ALD oxide to create patterns, images, and logos. These results show the use and commercial scale production of plasmonic systems for optical components and the potential for their integration with dynamically tunable media.

METHODS

Fabrication of Subwavelength Grating Arrays. Samples are fabricated on 8 in. diameter Eagle Glass wafers. A 200 nm layer of aluminum is sputtered on the surface followed by a 10 nm layer of silicon dioxide. Another aluminum deposition is performed to reach the desired resonator height, 110 nm. An opcial lithography is followed with etching of the aluminum ribs using an inductively coupled reactive ion etcher and the resist etch mask is removed with oxygen plasma.

Atomic Layer Deposition (ALD). ALD is performed using an Ultratech Savannah Gen 2 system. Zirconia is deposited using the tetrakis(dimethylamido)zirconium (TDMAZ) precursor and water. The reaction chamber is heated to 150 C. TDMAZ is heated to 75 C and pulsed for 0.15 s with water pulsed for 0.015 s. A relatively long purge time is used of 45 s for both TDMAZ and water due to the low process temperatures.

Optical Measurements and Images. Reflection spectra are collected using a 4×, 0.07 numerical aperture objective on an optical microscope coupled to a spectrometer (HR2000+, Ocean Optics). Reflection spectra are normalized to an aluminum mirror with 96% reflectivity and a linear polarizer. Images are collected using the same optical microscope with an Infinity 2-5 camera.

Finite Difference Time Domain Modeling. Reflection spectra are calculated using FIB obtained parameters with commercial finite-difference time-domain (FDTD) software package (Lumerical FDTD, Lumerical Solutions Inc.). The wavelength-dependent refractive index of aluminum is taken from Palik and the dispersion of ZrO_2 is obtained through ellipsometry, as shown in Figure S1.

ASSOCIATED CONTENT

Supporting Information

The Supporting Information is available free of charge on the ACS Publications website at DOI: 10.1021/acsanm.8b01147.

Refractive index and growth rate of ALD deposited ZrO_2 (PDF)

AUTHOR INFORMATION

Corresponding Authors

*(D.F.) E-mail Dan.Franklin@northwestern.edu.
*(D.C.) E-mail Debashis.Chanda@ucf.edu.

ORCID

Daniel Franklin: 0000-0002-6453-5114

Author Contributions

D.F. conceived the idea and designed experiments. D.F, M.G., and J.F. performed the experiments. D.F. analyzed and

DOI: 10.1021/acsanm.8b01147
ACS Appl. Nano Mater. XXXX, XXX, XXX–XXX

simulated the data. D.C. contributed materials/analysis tools. D.F. wrote and D.C. edited the paper.

Notes

The authors declare no competing financial interest.

■ ACKNOWLEDGMENTS

This work at University of Central Florida was supported by NSF Grant ECCS-1509729. The authors thank MOXTEK, Inc., for their expertise and support.

■ REFERENCES

(1) Kumar, K.; Duan, H. G.; Hegde, R. S.; Koh, S. C. W.; Wei, J. N.; Yang, J. K. W. Printing colour at the optical diffraction limit. *Nat. Nanotechnol.* **2012**, *7* (9), 557−561.
(2) Massenot, S.; Chevallier, R.; de la Tocnaye, J. L. D.; Parriaux, O. Tunable grating-assisted surface plasmon resonance by use of nano-polymer dispersed liquid crystal electro-optical material. *Opt. Commun.* **2007**, *275* (2), 318−323.
(3) Franklin, D.; Chen, Y.; Vazquez-Guardado, A.; Modak, S.; Boroumand, J.; Xu, D.; Wu, S. T.; Chanda, D. Polarization-independent actively tunable colour generation on imprinted plasmonic surfaces. *Nat. Commun.* **2015**, *6*, 7337.
(4) Franklin, D.; Frank, R.; Wu, S. T.; Chanda, D. Actively addressed single pixel full-colour plasmonic display. *Nat. Commun.* **2017**, *8*, 15209.
(5) Shao, L.; Zhuo, X.; Wang, J. Advanced Plasmonic Materials for Dynamic Color Display. *Adv. Mater.* **2018**, *30*, 1704338.
(6) Gordon, J. A.; Ziolkowski, R. W. Colors generated by tunable plasmon resonances and their potential application to ambiently illuminated color displays. *Solid State Commun.* **2008**, *146* (5−6), 228−238.
(7) Lee, Y.; Park, M. K.; Kim, S.; Shin, J. H.; Moon, C.; Hwang, J. Y.; Choi, J. C.; Park, H.; Kim, H. R.; Jang, J. E. Electrical Broad Tuning of Plasmonic Color Filter Employing an Asymmetric-Lattice Nanohole Array of Metasurface Controlled by Polarization Rotator. *ACS Photonics* **2017**, *4* (8), 1954−1966.
(8) Xu, T.; Walter, E. C.; Agrawal, A.; Bohn, C.; Velmurugan, J.; Zhu, W.; Lezec, H. J.; Talin, A. A. High-contrast and fast electrochromic switching enabled by plasmonics. *Nat. Commun.* **2016**, *7*, 10479.
(9) Kim, J. Y.; Kim, H.; Kim, B. H.; Chang, T.; Lim, J.; Jin, H. M.; Mun, J. H.; Choi, Y. J.; Chung, K.; Shin, J.; Fan, S.; Kim, S. O. Highly tunable refractive index visible-light metasurface from block copolymer self-assembly. *Nat. Commun.* **2016**, *7*, 12911.
(10) Lumdee, C.; Toroghi, S.; Kik, P. G. Post-fabrication voltage controlled resonance tuning of nanoscale plasmonic antennas. *ACS Nano* **2012**, *6* (7), 6301−7.
(11) Song, M. W.; Li, X.; Pu, M. B.; Guo, Y. H.; Liu, K. P.; Yu, H. L.; Ma, X. L.; Luo, X. G. Color display and encryption with a plasmonic polarizing metamirror. *Nanophotonics* **2018**, *7* (1), 323−331.
(12) Kim, S. J.; Kang, J. H.; Mutlu, M.; Park, J.; Park, W.; Goodson, K. E.; Sinclair, R.; Fan, S.; Kik, P. G.; Brongersma, M. L. Anti-Hermitian photodetector facilitating efficient subwavelength photon sorting. *Nat. Commun.* **2018**, *9* (1), 316.
(13) Xue, J.; Zhou, Z. K.; Wei, Z.; Su, R.; Lai, J.; Li, J.; Li, C.; Zhang, T.; Wang, X. H. Scalable, full-colour and controllable chromotropic plasmonic printing. *Nat. Commun.* **2015**, *6*, 8906.
(14) Yin, H.; Dong, B.; Liu, X.; Zhan, T.; Shi, L.; Zi, J.; Yablonovitch, E. Amorphous diamond-structured photonic crystal in the feather barbs of the scarlet macaw. *Proc. Natl. Acad. Sci. U. S. A.* **2012**, *109* (27), 10798−801.
(15) Saranathan, V.; Forster, J. D.; Noh, H.; Liew, S. F.; Mochrie, S. G.; Cao, H.; Dufresne, E. R.; Prum, R. O. Structure and optical function of amorphous photonic nanostructures from avian feather barbs: a comparative small angle X-ray scattering (SAXS) analysis of 230 bird species. *J. R. Soc., Interface* **2012**, *9* (75), 2563−80.
(16) McCoy, D. E.; Feo, T.; Harvey, T. A.; Prum, R. O. Structural absorption by barbule microstructures of super black bird of paradise feathers. *Nat. Commun.* **2018**, *9* (1), 1.
(17) Takeoka, Y. Angle-independent structural coloured amorphous arrays. *J. Mater. Chem.* **2012**, *22* (44), 23299−23309.
(18) Han, J.; Lee, E.; Dudoff, J. K.; Bagge-Hansen, M.; Lee, J. R. I.; Pascall, A. J.; Kuntz, J. D.; Willey, T. M.; Worsley, M. A.; Han, T. Y. J. Tunable Amorphous Photonic Materials with Pigmentary Colloidal Nanostructures. *Adv. Opt. Mater.* **2017**, *5* (7), 1600838.
(19) Lee, I.; Kim, D.; Kal, J.; Baek, H.; Kwak, D.; Go, D.; Kim, E.; Kang, C.; Chung, J.; Jang, Y.; Ji, S.; Joo, J.; Kang, Y. Quasi-amorphous colloidal structures for electrically tunable full-color photonic pixels with angle-independency. *Adv. Mater.* **2010**, *22* (44), 4973−7.
(20) Ye, M.; Sun, L.; Hu, X.; Shi, B.; Zeng, B.; Wang, L.; Zhao, J.; Yang, S.; Tai, R.; Fecht, H. J.; Jiang, J. Z.; Zhang, D. X. Angle-insensitive plasmonic color filters with randomly distributed silver nanodisks. *Opt. Lett.* **2015**, *40* (21), 4979−82.
(21) Teperik, T. V.; de Abajo, F. J. G.; Borisov, A. G.; Abdelsalam, M.; Bartlett, P. N.; Sugawara, Y.; Baumberg, J. J. Omnidirectional absorption in nanostructured metal surfaces. *Nat. Photonics* **2008**, *2* (5), 299−301.
(22) Galinski, H.; Favraud, G.; Dong, H.; Totero Gongora, J. S.; Favaro, G.; Döbeli, M.; Spolenak, R.; Fratalocchi, A.; Capasso, F. Scalable, ultra-resistant structural colors based on network metamaterials. *Light: Sci. Appl.* **2016**, *6* (5), e16233.
(23) Li, Z. Y.; Butun, S.; Aydin, K. Large-Area, Lithography-Free Super Absorbers and Color Filters at Visible Frequencies Using Ultrathin Metallic Films. *ACS Photonics* **2015**, *2* (2), 183−188.
(24) Mao, K.; Shen, W.; Yang, C.; Fang, X.; Yuan, W.; Zhang, Y.; Liu, X. Angle Insensitive Color Filters in Transmission Covering the Visible Region. *Sci. Rep.* **2016**, *6*, 19289.
(25) Yang, C.; Shen, W.; Zhang, Y.; Li, K.; Fang, X.; Zhang, X.; Liu, X. Compact multilayer film structure for angle insensitive color filtering. *Sci. Rep.* **2015**, *5*, 9285.
(26) Chung, D.; Shin, C.; Song, B.; Jung, M.; Yun, Y.; Nam, S. H.; Noh, C.; Kim, J.; Lee, S. Color filters for reflective display with wide viewing angle and high reflectivity based on metal dielectric multilayer. *Appl. Phys. Lett.* **2012**, *101* (22), 221120.
(27) Lee, K. T.; Han, S. Y.; Park, H. J. Omnidirectional Flexible Transmissive Structural Colors with High-Color-Purity and High-Efficiency Exploiting Multicavity Resonances. *Adv. Opt. Mater.* **2017**, *5*, 1700284.
(28) Lee, K. T.; Seo, S.; Guo, L. J. High-Color-Purity Subtractive Color Filters with a Wide Viewing Angle Based on Plasmonic Perfect Absorbers. *Adv. Opt. Mater.* **2015**, *3* (3), 347−352.
(29) Gu, Y.; Zhang, L.; Yang, J. K.; Yeo, S. P.; Qiu, C. W. Color generation via subwavelength plasmonic nanostructures. *Nanoscale* **2015**, *7* (15), 6409−19.
(30) Lee, K. T.; Jang, J. Y.; Park, S. J.; Ji, C.; Guo, L. J.; Park, H. J. Subwavelength nanocavity for flexible structural transmissive color generation with a wide viewing angle. *Optica* **2016**, *3* (12), 1489−1495.
(31) Laks, B.; Mills, D. L.; Maradudin, A. A. Surface-Polaritons on Large-Amplitude Gratings. *Phys. Rev. B: Condens. Matter Mater. Phys.* **1981**, *23* (10), 4965−4976.
(32) Le Perchec, J.; Quemerais, P.; Barbara, A.; Lopez-Rios, T. Why metallic surfaces with grooves a few nanometers deep and wide may strongly absorb visible light. *Phys. Rev. Lett.* **2008**, *100* (6), 066408.
(33) Lansey, E.; Hooper, I. R.; Gollub, J. N.; Hibbins, A. P.; Crouse, D. T. Light localization, photon sorting, and enhanced absorption in subwavelength cavity arrays. *Opt. Express* **2012**, *20* (22), 24226−36.
(34) Porto, J. A.; Garcia-Vidal, F. J.; Pendry, J. B. Transmission resonances on metallic gratings with very narrow slits. *Phys. Rev. Lett.* **1999**, *83* (14), 2845−2848.
(35) Lopez-Rios, T.; Mendoza, D.; Garcia-Vidal, F. J.; Sanchez-Dehesa, J.; Pannetier, B. Surface shape resonances in lamellar metallic gratings. *Phys. Rev. Lett.* **1998**, *81* (3), 665−668.

DOI: 10.1021/acsanm.8b01147
ACS Appl. Nano Mater. XXXX, XXX, XXX−XXX

(36) Sobnack, M. B.; Tan, W. C.; Wanstall, N. P.; Preist, T. W.; Sambles, J. R. Stationary surface plasmons on a zero-order metal grating. *Phys. Rev. Lett.* **1998**, *80* (25), 5667−5670.
(37) Kreiter, M.; Mittler, S.; Knoll, W.; Sambles, J. R. Surface plasmon-related resonances on deep and asymmetric gold gratings. *Phys. Rev. B: Condens. Matter Mater. Phys.* **2002**, *65* (12), 125415.
(38) Miyazaki, H. T.; Kurokawa, Y. Controlled plasmon resonance in closed metal/insulator/metal nanocavities. *Appl. Phys. Lett.* **2006**, *89* (21), 211126.
(39) Collin, S.; Pardo, F.; Pelouard, J. L. Waveguiding in nanoscale metallic apertures. *Opt. Express* **2007**, *15* (7), 4310−20.
(40) Guo, L.; Sun, Z. J. Analytical Determination of Plasmon Resonances in MIM Nanocavities. *Plasmonics* **2015**, *10* (6), 1625−1629.
(41) Chandran, A.; Barnard, E. S.; White, J. S.; Brongersma, M. L. Metal-dielectric-metal surface plasmon-polariton resonators. *Phys. Rev. B: Condens. Matter Mater. Phys.* **2012**, *85* (8), 085416.
(42) Wu, Y. K.; Hollowell, A. E.; Zhang, C.; Guo, L. J. Angle-insensitive structural colours based on metallic nanocavities and coloured pixels beyond the diffraction limit. *Sci. Rep.* **2013**, *3*, 1194.
(43) Fang, B.; Yang, C.; Shen, W.; Zhang, X.; Zhang, Y.; Liu, X. Highly efficient omnidirectional structural color tuning method based on dielectric-metal-dielectric structure. *Appl. Opt.* **2017**, *56* (4), C175−C180.
(44) Fang, Z. Y.; Zhen, Y. R.; Fan, L. R.; Zhu, X.; Nordlander, P. Tunable wide-angle plasmonic perfect absorber at visible frequencies. *Phys. Rev. B: Condens. Matter Mater. Phys.* **2012**, *85* (24), 245401.
(45) Vanderkolk, G. J.; Verkerk, M. J. Microstructural Studies of the Growth of Aluminum Films with Water Contamination. *J. Appl. Phys.* **1986**, *59* (12), 4062−4067.
(46) Wu, Y. K.; Hollowell, A. E.; Zhang, C.; Guo, L. J. Angle-insensitive structural colours based on metallic nanocavities and coloured pixels beyond the diffraction limit. *Sci. Rep.* **2013**, *3*, 1194.

DOI: 10.1021/acsanm.8b01147
ACS Appl. Nano Mater. XXXX, XXX, XXX−XXX